Supporting Information

From flat to deep concave: an unusual mode of facet control

Shenghao Yang,[a] Yonglong Zheng,[a] Guangyu He,[b] Mengmeng Zhang,[a] Hongyan Li,[a] Yawen Wang*[a] and Hongyu Chen*[ac]

[a] Institute of Advanced Synthesis (IAS), and School of Chemistry and Molecular Engineering, Jiangsu National Synergetic Innovation Centre for Advanced Materials, Nanjing Tech University, Nanjing, 211816, China.

[b] Research Institute of Zhejiang University-Taizhou, Taizhou, 318000, China.

[c] College of Science, Westlake University, Hangzhou, 310023, China. (Current)

*E-mail: ias_ywwang@njtech.edu.cn; chenhongyu@westlake.edu.cn

Experimental Section

Materials

All solutions were prepared using deionized water (resistivity > 18 MΩ·cm). Hydrogen tetrachloroaurate (III) tetrahydrate ($HAuCl_4 \cdot 4H_2O$, 49% metal basis, Alfa-Aesar), cetyltrimethylammonium bromide (CTAB, 99% Sigma-Aldrich), sodium borohydride ($NaBH_4$, 99%, Sigma-Aldrich), trisodium citrate dihydrate (CA, 99%, Alfa-Aesar), L-ascorbic acid (99%, Sigma-Aldrich), and L-cysteine (99%, Energy), 3-mercaptobenzoic acid (95%, Sigma-Aldrich), N-acetyl-L-cysteine (99%, Sigma-Aldrich), glycine (Sinopharm Chemical Reagent Co., Ltd.), serine (99%, Alfa-Aesar) and L-glutathione (98%, Sigma-Aldrich) was used as received.

Synthesis

Synthesis of concave Triangular Au nanoplate seeds. Triangular Au nanoplate seeds were synthesized according to a previously proposed protocol[1]. The as-synthesized nanoplates were directly used in the following synthesis. For the syntheses of 400 nm and 700 nm nanoplates, the seed solution added was decreased to 20 uL and 10 uL

respectively.

Synthesis of the hexagonal hollow particles. The whole process was performed in a 60℃ oven. A 5.0 mL growth solution containing 10 mM of CTAB, 0.15 mM of $HAuCl_4$ and 0.33 mM of L-ascorbic acid was first prepared and heated to 60 ℃, followed by addition of 40 uL of 0.01 mM L-cysteine. Next, 80 μL of triangular gold nanoplates solution was quickly added under vigorous vortexing. The reaction mixture was incubated at 60℃ for 30 min, and then air-cooled to room temperature. Further prolonging the incubation to 2 h would not change the morphology of the concave structures (Fig. S9). The product was purified with centrifugation and subjected to characterizations.

Characterization

TEM images were collected from a Talos L120C model operated at 120 kV. Field emission scanning electron microscopy (SEM) image were collected on a FEI Quanta 250 FEG model. High resolution TEM image and 3D tomography data were taken from a FEI Talos F200X Transmission Electron Microscope operated at 200 kV. The XRD analysis was carried out on a SmartLab TM X-ray diffractometer with Cu Kα radiation. SEM images of focused ion beam (FIB)-cut slices were collected by a TESCAN LYRA 3 XMU model.

First-Principles Calculations

Ab *initio* density functional theory (DFT) calculations are performed using the Quantum-ESPRESSO package.[2] The generalized gradient approximation (GGA) exchange-correlation functional proposed by Perdew, Burke and Ernzerhof (PBE) is employed. The wave functions and charge density are expanded with kinetic cutoffs of 60 and 600 Ry, respectively. Electron-ion interactions are described using ultrasoft pseudopotentials and relativistic effect is taken into consideration. The total energy is converged to within 1×10^{-4} Ry, and the geometry is optimized until the atomic force becomes less than 1×10^{-3} Ry·Bohr^{-1}. The long-range van der Waals (vdW) forces are explicitly included in the calculations by adding to the PBE functional the Grimme's

semiempirical correction term (DFT-D3).[3] Periodic boundary conditions are employed to model Au surfaces for three low-Miller-index planes, (100), (110) and (111). The lengths of the supercells are 8.16 Å × 8.16 Å, 8.16 Å × 11.54 Å, 5.77 Å × 9.99 Å for (100), (110) and (111) as shown in Fig S12. In all cases, model with four layers is adopted and the bottom two layers are kept fixed to mimic the bulk while the upper two layers are fully relaxed. A 15 Å vacuum layer is used along the z direction to avoid periodic interactions and a dipole correction is employed.[4] The isoelectric point of cysteine is 5.05 while the pH in experiment is range from 6 to 7, we investigate cysteine with COO^- and NH_2. Taking the well-known affinity between thiolate groups and gold[5] into consideration, we focus on cysteine with S^- as shown in Fig. S12.

All the adsorption energies (E_{ab}) are calculated using the following energy difference,

$$E_{ab} = E_{complex} - E_{absorbate} - E_{substrate}$$

where $E_{complex}$ represents the total energies of the system, $E_{adsorbate}$ and $E_{substrate}$ represent the energies of adsorbate and substrate, respectively.

Different adsorption configurations of L-cysteine on the Au surface are calculated (Fig. S10). The configuration with L-cysteine parallel to the surface of Au has the lowest adsorption energy on all three facets, and the -4.73 eV adsorption energy of L-cysteine on Au(110) is distinctly larger than those on the other surfaces, consistent with the facet specificity.[6] The detailed adsorption configurations were also surveyed, and the calculated Au-S and Au-O distances of L-cysteine on Au(110) are 2.36 Å and 2.24 Å, while on Au(100) the distances are 2.36 Å and 2.32 Å, and on Au(111) are 2.45 Å and 2.53 Å. Thus, the ligand is closer and more tightly bound to the Au(110). The apparent differences in adsorption energies might be attributed to the loose lattice structure of Au(110) (Fig. S11), which can better align with L-cysteine ligand, while the tight lattice structure of Au(111) has the opposite effect and thus the lowest adsorption energy for L-cysteine.

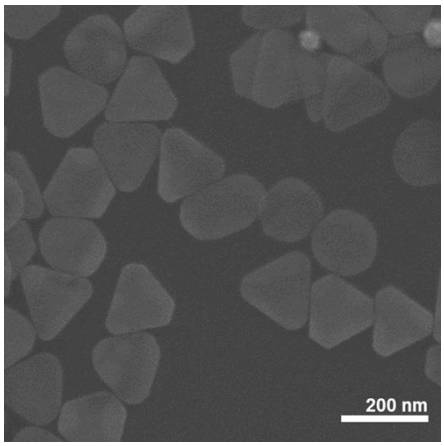

Fig. S1 SEM image of the triangular Au nanoplates.

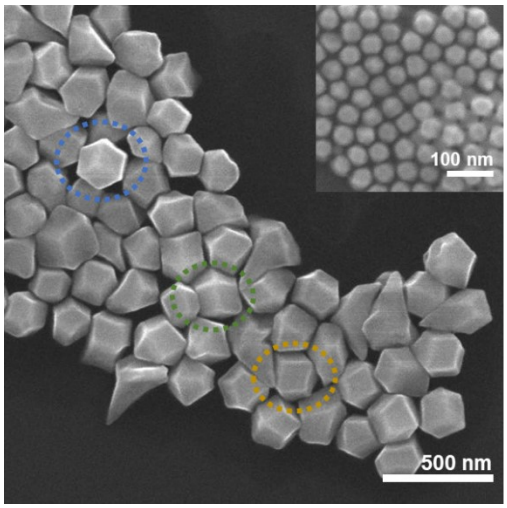

Fig. S2 SEM images of the octahedral Au seeds and rhombic dodecahedron particles when octahedral Au nanoparticles as seeds.

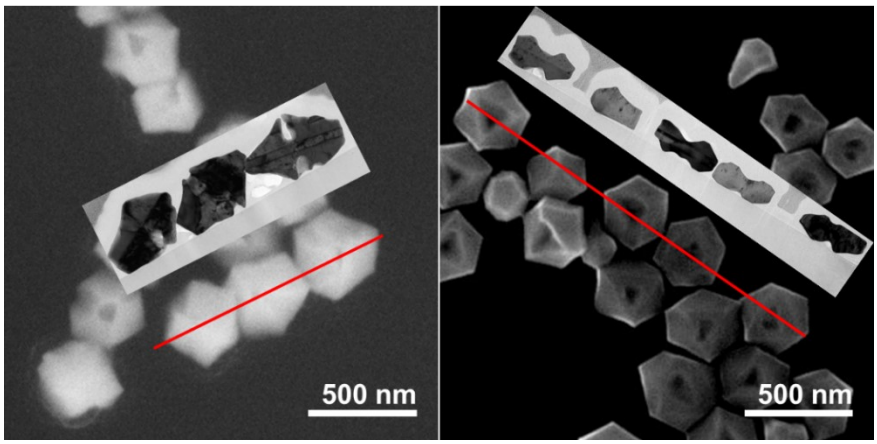

Fig. S3 SEM images of the particles cut by the focused-ion beam across the centers (with the red line indicated the cutting line) and the TEM images of respective slices.

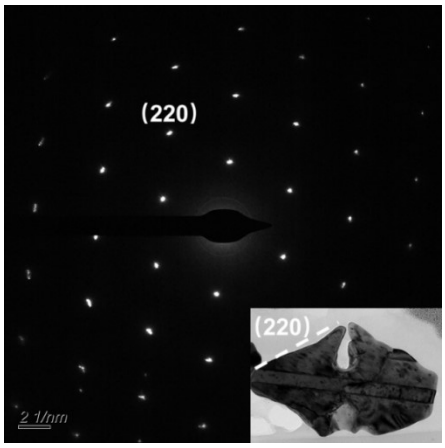

Fig. S4 The adding SAED pattern data of the opening part of the hexagonal bowls.

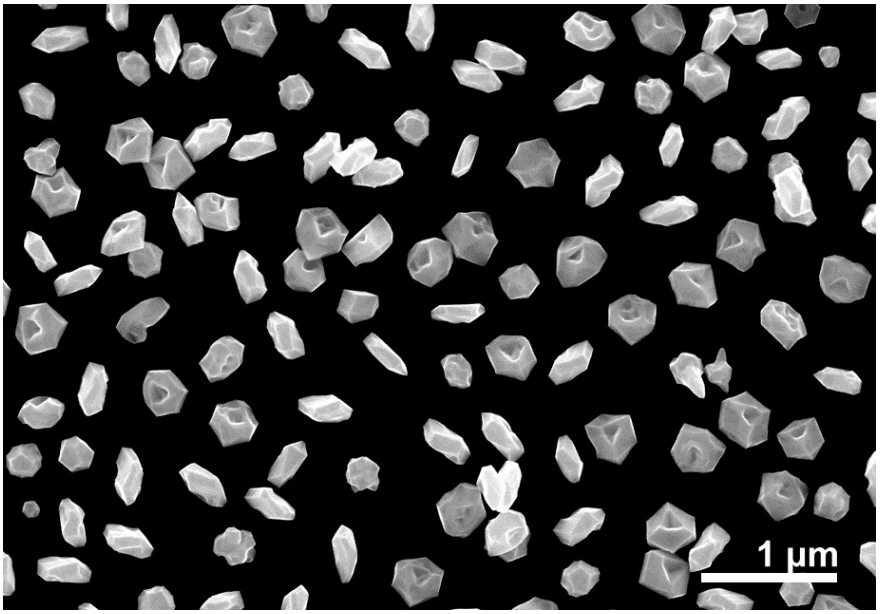

Fig. S5 SEM image of the concaved hexagonal bowls with different orientations. The side-view of the particles revealed two different types of the particles.

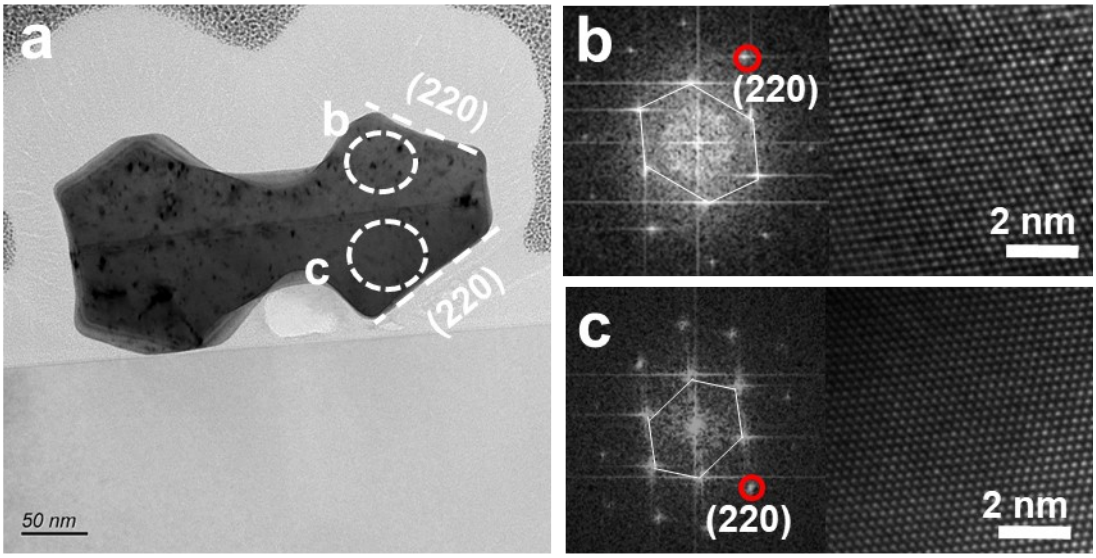

Fig. S6 TEM image (a) of a FIB-cut slice in a particle with one twining plane; HRTEM images and corresponding FFT patterns of its top (b) and bottom (c) blocks.

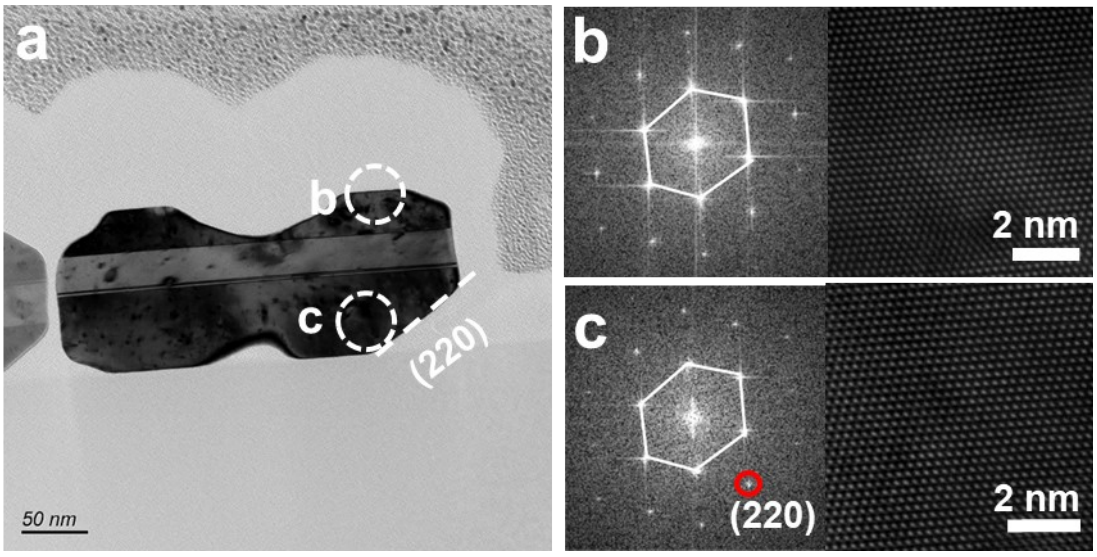

Fig. S7 TEM image (a) of a FIB-cut slice in a particle with two twining planes; HRTEM images and corresponding FFT patterns of its top (b) and bottom (c) blocks.

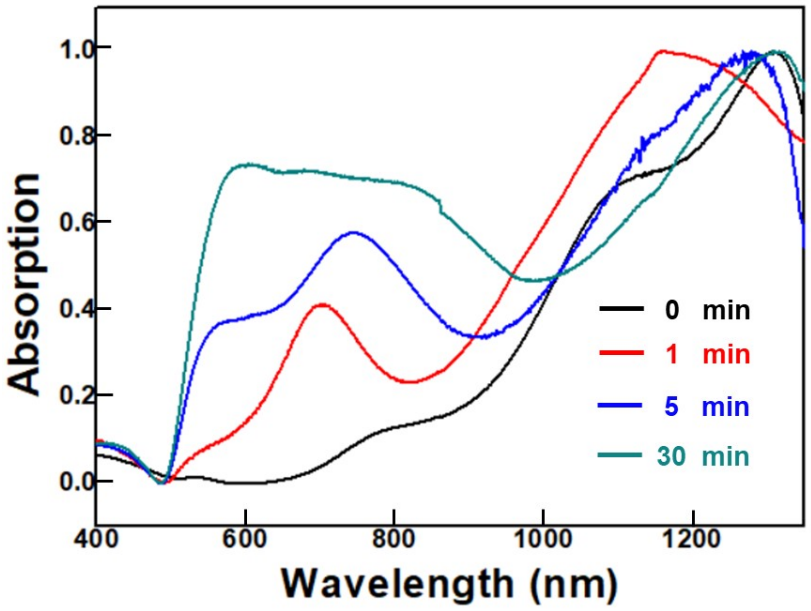

Fig. S8 The ultraviolet data of the time-dependent evolution of the hexagonal bowls at 0 min, 1 min, 5 min, and 30 min reaction time.

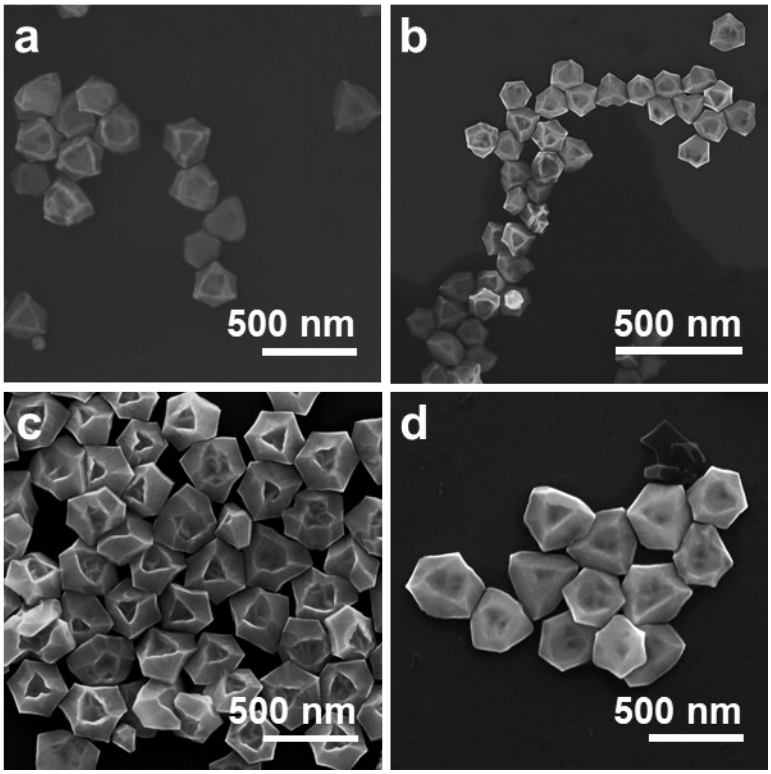

Fig. S9 The large view SEMINAR images and corresponding yields of the time-dependent evolution of the hexagonal bowls at a) 1min (yield=86%), b) 5min (yield=93%), c) 30min (yield=95%) and 2 hours (yield=95%). Most of the impurities are nanoparticles formed by homogeneous nucleation.

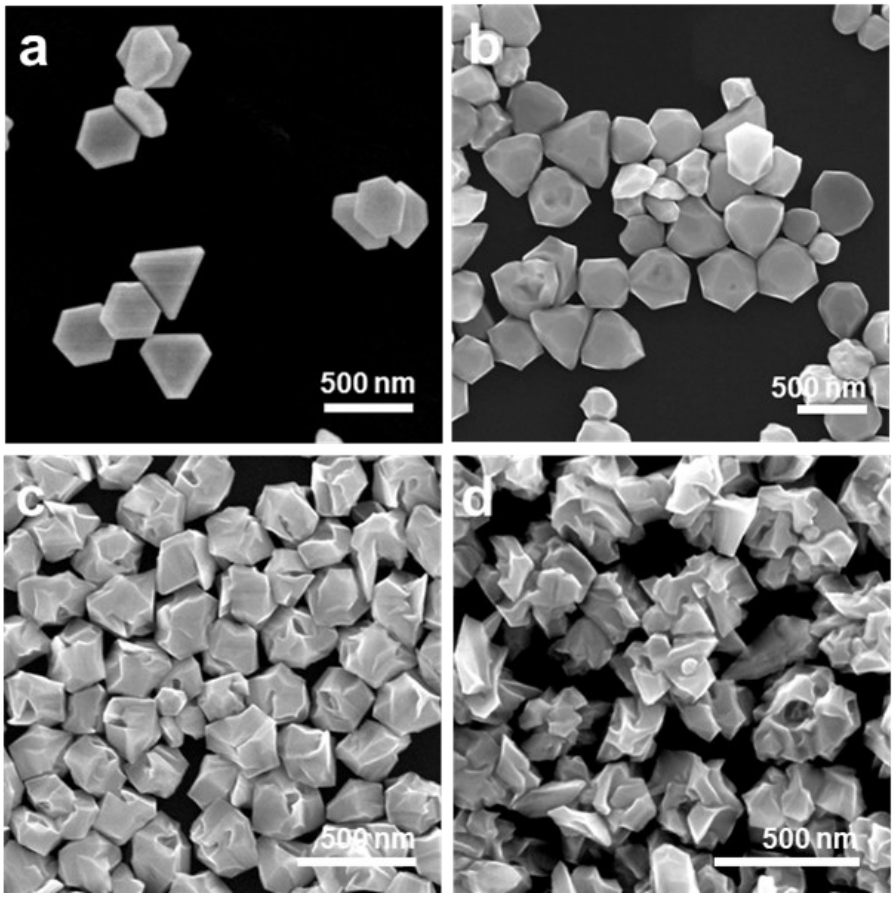

Fig. S10 SEM images of the nanostructures formed a) without L-cysteine, and with b) 0.02 μM, c) 0.10 μM and d) 0.24 μM L-cysteine.

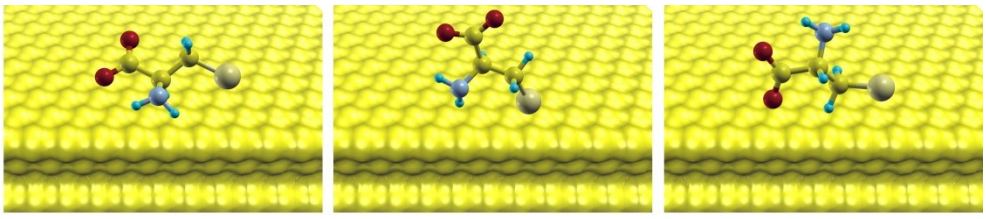

Au(100)	-2.59 eV	-2.31 eV	-2.43 eV
Au(110)	-4.73 eV	-4.63 eV	-4.49 eV
Au(111)	-1.24 eV	-0.63 eV	-0.59 eV

Fig. S11 The adsorption energies of L-cysteine on Au(100), Au(110) and Au(111) with different configurations.

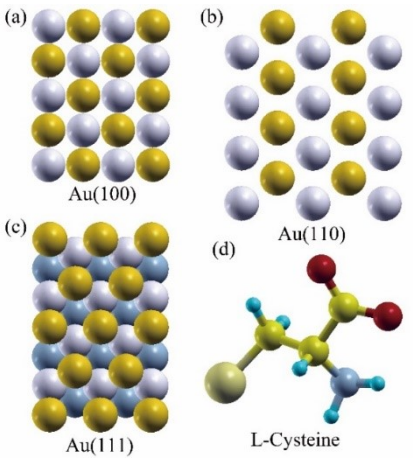

Fig. S12 (a)-(c) different lattice planes of Au, yellow = the first layer, white = the second layer, blue = the third layer. (d) Optimized structure of L-cysteine, yellow = C, wathet blue = H, red = O, blue = N and pale yellow = S.

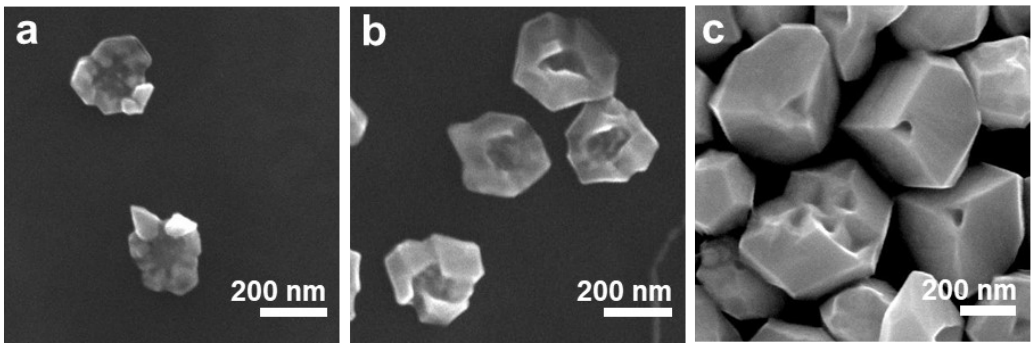

Fig. S13 SEM images of the nanostructures formed with a) 0.025 mM, b) 0.050 mM, and c) 0.25 mM $HAuCl_4$.

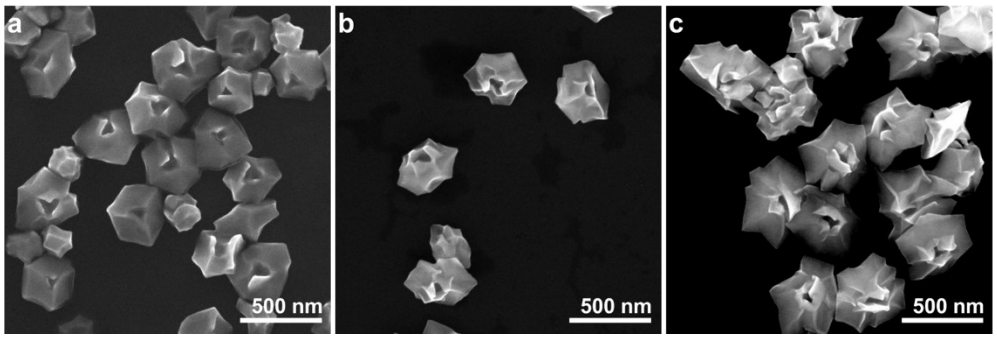

Fig. S14 SEM images of the concaved bowls formed with a) 1mM, b) 4mM and c)10 mM L-ascorbic acid.

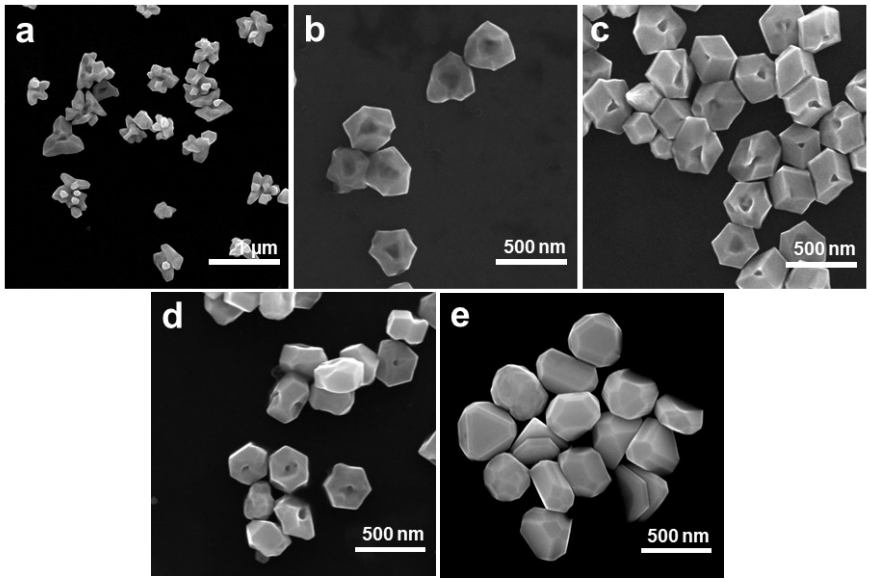

Fig. S15 SEM images of the nanostructures formed with a) 2.0 mM, b) 5.0 mM, c) 15 mM d) 100 mM, and e) 200 mM CTAB.

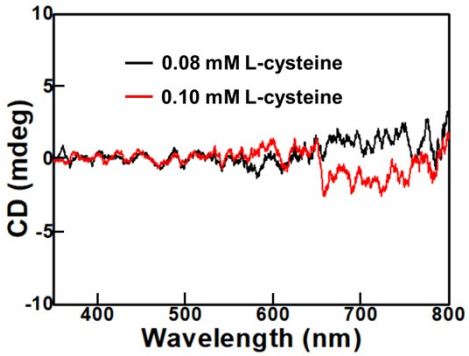

Fig. S16 CD spectra of the corresponding samples formed with different concentration of L-cysteine.

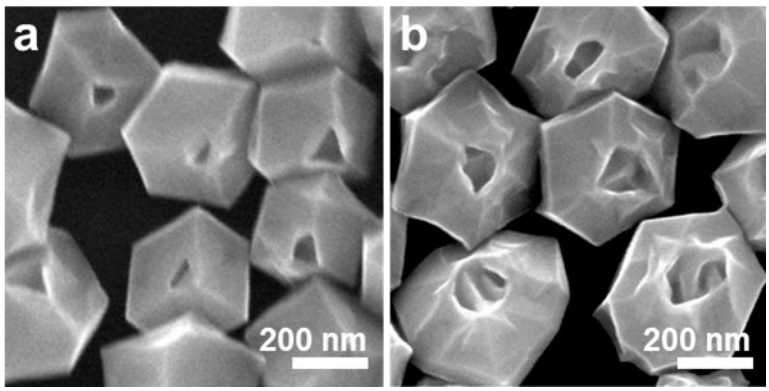

Fig. S17 SEM images of the nanostructures formed by replacing the L-cysteine with (a) D-cysteine and (b) DL-cysteine.

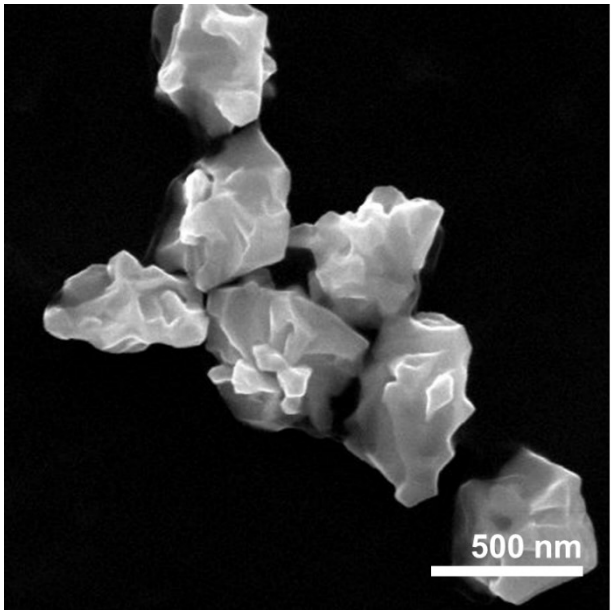

Fig. S18 SEM image of the concaved bowls using pre-formed concaved bowls as the seeds for another round of growth.

Table S1 Comparison of the ligand and precursor concentrations with chiral growths employing the CTAB/L-cysteine ligand system.

	Nam Group[7]	Wu Group[8]	Wong Group[9]	This Work
CTAB/CTAC (mM)	14.6	10	28.2	10
$HAuCl_4$ (mM)	0.365	0.1	0.19	0.15
L-cysteine (μM)	$9.12x10^{-2}$	20	$4x10^{-2}$	$8x10^{-2}$

References

1. Y. Huang, A. R. Ferhan, Y. Gao, A. Dandapat and D.-H. Kim, High-yield Synthesis of Triangular Gold Nanoplates with Improved Shape Uniformity, Tunable Edge Length and Thickness, *Nanoscale* **2014**, *6*, 6496-6500.
2. P. Giannozzi, S. Baroni, N. Bonini, M. Calandra, R. Car, C. Cavazzoni, D. Ceresoli, G. L. Chiarotti, M. Cococcioni, S. Fabris and *et al*, QUANTUM ESPRESSO: A Modular and Open-Source Software Project for Quantum Simulations of Materials, *Journal of Physics: Condensed Matter* **2009,** *21*, 395502.
3. S. Grimme, Semiempirical GGA-Type Density Functional Constructed with a Long-Range Dispersion Correction, *Journal of Computational Chemistry* **2006,** *27*, 1787-1799.
4. L. Bengtsson, Dipole Correction for Surface Supercell Calculations. *PHYSICAL REVIEW B* **1999,** *59*.
5. H. Häkkinen, The Gold–Sulfur Interface at the Nanoscale. *Nature Chemistry* **2012,**

4, 443-455.
6. J. Morales-Vidal, N. López and M. A. Ortuño, Chirality Transfer in Gold Nanoparticles by l-Cysteine Amino Acid: A First-Principles Study, *The Journal of Physical Chemistry C* **2019**, *123*, 13758-13764.
7. H.-E. Lee, H.-Y. Ahn, J. Mun, Y. Y. Lee, M. Kim, N. H. Cho, K. Chang, W. S. Kim, J. Rho and K. T. Nam, Amino-Acid- and Peptide-Directed Synthesis of Chiral Plasmonic Gold Nanoparticles, *Nature* **2018**, *556*, 360-365.
8. Yan, Y. Chen, S. Hou, J. Chen, D. Meng, H. Zhang, H. Fan, Y. Ji and X. Wu, Fabricating Chiroptical Starfruit-Like Au Nanoparticles via Interface Modulation of Chiral Thiols, *Nanoscale* **2017**, *9*, 11093-11102.
9. G. Zheng, Z. Bao, J. Pérez-Juste, R. Du, W. Liu, J. Dai, W. Zhang, L. Y. S. Lee and K.-Y. Wong, Tuning the Morphology and Chiroptical Properties of Discrete Gold Nanorods with Amino Acids, *Angew. Chem. Int. Ed.* **2018**, *57*, 16452-16457.